

# STRANGE ATTRACTORS IN A PERIODICALLY PERTURBED LORENZ-LIKE EQUATION\*

Fengjuan Chen<sup>†</sup> and Liqun Zhou

**Abstract** This paper studies a periodically perturbed Lorenz-like equation. We obtain three types of attractors: (i) periodic sinks, (ii) Hénon-like attractors, and (iii) rank one attractors. Among the three, (i) represent the stable dynamics of equation, and (ii) and (iii) represent chaotic behaviors characterized by an Sinai-Ruelle-Bowen(SRB) measure. Each attractor admits a basin of positive Lebesgue measure, hence we observe it in numerical simulations.

**Keywords** Homoclinic tangle, Hénon-like attractor, rank one attractor, SRB measure.

**MSC(2000)** 37D45, 37C40.

## 1. Introduction

One main theme in dynamical system is to understand the complicated behaviors of differential equations. Chaos, characterized by sensitivity of initial state, have a long history of research. In 1890, Poincaré discovered homoclinic tangles during the study of three-body problem. Since then, many theories and methods have been developed to verify chaos, such as the Birkhoff-Smale homoclinic theorem and Melnikov method. Later, from ergodic point of view, chaos means the existence of an invariant measure with good mixing properties. If a system admits an Sinai-Ruelle-Bowen(SRB) measure [8] supported on a set with positive Lebesgue measure, one can not only justify chaos rigorously but also observe the chaotic attractors from numerical simulations. Hénon attractor is such an example with SRB measure on  $D \subset \mathbb{R}^2$  [2].

The Lorenz equations have a chaotic attractor at certain parameters. The mechanism of onset the chaotic Lorenz attractor interests many researchers. Whether there is an invariant measure featuring the Lorenz attractor. This paper investigates a Lorenz-like equation. With the homoclinic tangle theory developed by Wang and Oksasoglu in [5, 6], three types of attractors are created for the periodically perturbed Lorenz-like equation. One type is the periodic sinks, dedicated by atomic measures, representing asymptotically stable dynamics. The other two types are Hénon-like attractors and rank one attractors, dedicated by SRB measures, representing chaotic behaviors of equation. Since the basins are with positive Lebesgue measure, all the three types of attractors are observed in numerical simulations.

<sup>†</sup>the corresponding author. Email address: [fjchen@zjnu.cn](mailto:fjchen@zjnu.cn)(F. Chen)

College of Mathematics, Physics and Information Engineering, Zhejiang Normal University, Jinhua 321004, China

\*The authors were supported by National Natural Science Foundation of China (11171309).

## 2. Two-dimensional homoclinic tangle theory

Although homoclinic tangle was discovered earlier by Poincaré in 1890, the overall dynamical structure is far from understood beyond horseshoe. Recently, Wang and Oksasoglu provided a systematic study on homoclinic tangles for a second-order equation [5]:

$$\begin{aligned}\frac{dx}{dt} &= f(x, y), \\ \frac{dy}{dt} &= g(x, y),\end{aligned}\tag{2.1}$$

where  $f(x, y)$ ,  $g(x, y)$  are  $C^r$  ( $r \geq 3$ ) functions on  $V \subset \mathbb{R}^2$ . Equation (2.1) has a saddle point  $O$  and one homoclinic solution  $\ell(t)$ . Assume that  $O$  is dissipative. Consider the periodic perturbation to Eq.(2.1):

$$\begin{aligned}\frac{dx}{dt} &= f(x, y) + \mu P(x, y, t), \\ \frac{dy}{dt} &= g(x, y) + \mu Q(x, y, t),\end{aligned}\tag{2.2}$$

where  $P(x, y, t)$ ,  $Q(x, y, t)$  are also  $C^r$  functions, and periodic in  $t$  of  $T$ .  $\mu$  is the magnitude of perturbation.

Usually, the homoclinic solution  $\ell(t)$  is broken, leading to homoclinic tangles and horseshoes. However, there is a possibility that stable and unstable manifolds are pulling apart. Define [5]

$$\mathcal{W}(\theta) = \int_{-\infty}^{\infty} [P(\ell(t), t + \theta), Q(\ell(t), t + \theta)] \cdot \tau_{\ell(t)}^{\perp} e^{-\int_0^t E_{\ell}(s) ds} dt \tag{2.3}$$

as the Melnikov function, where  $\tau_{\ell(t)}^{\perp}$  is a vector perpendicular to the tangent vector of  $\ell(t)$  at time  $t$ , and  $E_{\ell}(t)$  is the expansion rate of solutions in the neighborhood of  $\ell(t)$ . Denote

$$M = \max_{\theta \in S^1} \mathcal{W}(\theta), \quad m = \min_{\theta \in S^1} \mathcal{W}(\theta), \tag{2.4}$$

where  $S^1 = [nT, (n+1)T)$  for  $n = 0, 1, 2, \dots$ .

**Theorem 2.1.** (*[5]*) *Assume that  $\mathcal{W}(\theta)$  is a Morse function.*

- (I) *If  $m < 0 < M$ , then horseshoes, periodic sinks, and Hénon-like attractors are created in the neighborhood of  $\ell(t)$ . Moreover, as  $\mu \rightarrow 0$ , the three dynamical phenomena repeat with period  $e^{\lambda T}$ , where  $\lambda$  is the unstable eigenvalue of saddle  $O$ .*
- (II) *If  $m > 0$ , then the stable and unstable manifolds are pulled apart. Therefore, rank one attractors with SRB measures are generated for large  $\omega$ , where  $\omega$  is the frequency of perturbation.*

Theorem 2.1 grounds on one homoclinic solution with a dissipative saddle point. Instead of one homoclinic solution, if *two homoclinic solutions* connect a dissipative saddle point of Eq.(2.1), then dynamics is critically different. In this case, we have two Melnikov functions associated with two homoclinic solutions. In terms

of four extrema of two Melnikov functions, five types of attractors will arise in the neighborhood of two homoclinic solutions.

Let  $\mathcal{W}^+(\theta)$  and  $\mathcal{W}^-(\theta)$  be two Melnikov functions. Denote

$$\begin{aligned} M^+ &= \max_{\theta \in S^1} \mathcal{W}^+(\theta), & m^+ &= \min_{\theta \in S^1} \mathcal{W}^+(\theta), \\ M^- &= \max_{\theta \in S^1} \mathcal{W}^-(\theta), & m^- &= \min_{\theta \in S^1} \mathcal{W}^-(\theta). \end{aligned} \quad (2.5)$$

**Theorem 2.2.** (*[7]*) *Assume that  $\mathcal{W}^+(\theta)$  and  $\mathcal{W}^-(\theta)$  are two Morse functions.*

- (i) *If  $m^+, m^- < 0 < M^+, M^-$ , then Eq.(2.2) shows the mixture of two homoclinic tangles. It contains periodic sinks, Hénon-like attractors, and rank one attractors.*
- (ii) *If  $m^+ < 0 < M^+$ ,  $m^- > 0$  (or  $m^- < 0 < M^-$ ,  $m^+ > 0$ ), then Eq.(2.2) shows one homoclinic tangle and one rank one attractor. One-sided periodic sinks, one-sided Hénon-like attractors, and one-sided rank one attractors are created.*
- (iii) *If  $m^+ < 0 < M^+$ ,  $M^- < 0$  (or  $m^- < 0 < M^-$ ,  $M^+ < 0$ ), then Eq.(2.2) shows one tangle mixed with one rank one attractor. Periodic sinks, Hénon-like attractors, and rank one attractors, including two-sided and one-sided, are permitted.*
- (iv) *If  $M^+ < 0$ ,  $M^- < 0$  (or  $M^+ < 0$ ,  $m^- > 0$  or  $M^- < 0$ ,  $m^+ > 0$ ), then Eq.(2.2) shows one rank one attractor.*
- (v) *If  $m^+ > 0$ ,  $m^- > 0$ , then Eq.(2.2) shows two rank one attractors.*

As  $\mu \rightarrow 0$ , each dynamical pattern of the five types repeats itself with period  $e^{\lambda T}$ , where  $\lambda$  is the unstable eigenvalue of  $O$ .

The proof of theorem 2.1 and theorem 2.2 depend on an one-dimensional singular limit circle map. Both the limit maps have non-degenerate critical points, which induce the complicated dynamics. With the non-uniformly hyperbolic theory, the return map in extended phase space admits all the invariant sets in theorem 2.1 and theorem 2.2. In fact, the distribution of orbits starting from the neighborhood of homoclinic solutions are dedicated by an invariant measure. Let  $F$  be the return map, and  $\nu$  be the invariant measure. Then there is a set  $U$  having positive Lebesgue measure such that for every continuous functions  $\varphi : U \rightarrow R$  and every  $x \in U$ , we have

$$\frac{1}{n} \sum_{i=0}^{n-1} \varphi(F^i x) \rightarrow \int \varphi d\nu. \quad (2.6)$$

The invariant measure  $\nu$  in (2.6) is the SRB measure [8]. From (2.6), horseshoes are negligible in measure theoretic sense. However, periodic sinks, Hénon-like attractors, and rank one attractors are with the attractive basin of positive measure, hence observable in simulations.

Given a three-dimensional equation, also possessing a dissipative saddle point and homoclinic solutions. Do theorem 2.1 and theorem 2.2 hold yet? If hold, what kind of attractors will arise? Do they still repeat with certain period? We explore, through a Lorenz-like equation, the homoclinic tangle theory in three-dimensional differential equations.

### 3. Dynamics of periodically perturbed Lorenz-like equation

#### 3.1. Theoretical analysis

We start with a Lorenz-like equation [1, 3]:

$$\begin{aligned}\frac{dx}{dt} &= \beta(x - y), \\ \frac{dy}{dt} &= -4\beta y + xz + \varepsilon x^3, \\ \frac{dz}{dt} &= -\alpha\beta z + xy + \delta z^2,\end{aligned}\tag{3.1}$$

where  $\beta > 1$ ,  $\alpha > 0$ ,  $\delta$ , and  $\varepsilon$  are parameters. Equation (3.1) acts an interesting model to optical effects in nematic-liquid-crystal films [3]. If  $\delta = 0$  and  $x^3$  is  $x$ , Eq.(3.1) turns to the famous Lorenz equation.

Evidently, Eq.(3.1) has an equilibrium point  $O(0, 0, 0)$ . The eigenvalues are

$$\lambda_1 = \beta, \lambda_2 = -4\beta, \lambda_3 = -\alpha\beta.\tag{3.2}$$

$\beta > 1$  and  $\alpha > 0$  lead to  $\lambda_1 > 0$ ,  $\lambda_2 < 0$ , and  $\lambda_3 < 0$ . So  $\lambda_1 + \lambda_2 + \lambda_3 < 0$ , hence  $O(0, 0, 0)$  is a dissipative saddle point. Reference [3] reported the first gluing bifurcation happening at  $\beta = 1.8$ ,  $\alpha = 1.5$ ,  $\delta = -0.07$ , and  $\varepsilon = 0.076071$ . At these values, we find the double homoclinic solutions to saddle  $O(0, 0, 0)$ ; see Fig.1.

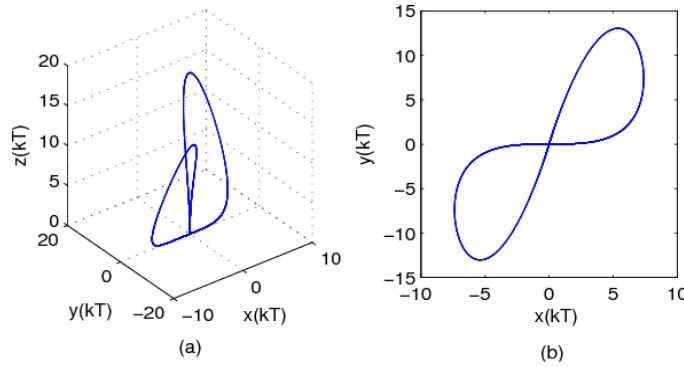


Figure 1. Double homoclinic solutions of Eq.(3.1) at  $\beta = 1.8$ ,  $\alpha = 1.5$ ,  $\delta = -0.07$ ,  $\varepsilon = 0.076071148687$ . (a) Three-dimensional phase portrait; (b) Projection on  $x - y$  plane.

Consider the periodically perturbation to Eq.(3.1):

$$\begin{aligned}\frac{dx}{dt} &= \beta(x - y) + \mu \sin \omega t, \\ \frac{dy}{dt} &= -4\beta y + xz + \varepsilon x^3, \\ \frac{dz}{dt} &= -\alpha\beta z + xy + \delta z^2,\end{aligned}\tag{3.3}$$

where  $\mu$  and  $\omega$  are parameters. From homoclinic tangle theory of two-dimensional differential equations [7], we expect three types of attractors arising from double homoclinic tangles. Figure 2 is bifurcation diagram of Eq.(3.3) with respect to the parameter  $\mu$ . From Fig.2, Eq.(3.3) have both chaotic and periodic motions in an intermittent way. However, what is the mechanism of these motions.

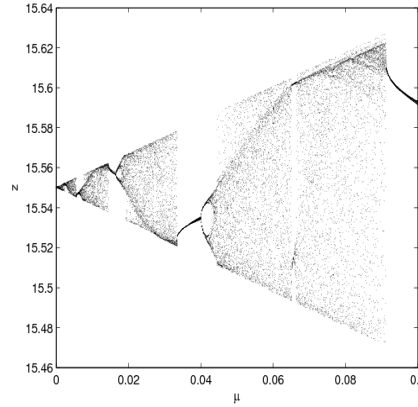


Figure 2. Bifurcation diagram of equation (3.3) with respect to  $\mu$  at  $\beta = 1.8, \alpha = 1.5, \delta = -0.07$  and  $\varepsilon = 0.076071148687$ .

## 3.2. Numerical simulations

In this section, we do numerical experiment to find all the attractors for Eq.(3.3) when  $\mu$  varies in  $(0, 0.1)$ . We take the viewpoint that observable events correspond to positive Lebesgue measure sets.

### 3.2.1. Simulation procedure

(i) First we fix parameters  $(\beta, \alpha, \delta) = (1.8, 1.5, -0.07)$ . Then, using the fourth-order Runge-Kutta routine, we numerically integrate Eq.(3.1) to find the corresponding value of  $\varepsilon$  for double homoclinic solutions at initial point  $(x_0, y_0, z_0) = (0.01, 0, 0)$ . This initial point is fixed throughout. Since  $\mu$  reaches  $10^{-8}$  in magnitude in simulations, we calculate the value of  $\varepsilon$  up to the precision of  $10^{-12}$ . Figure 1 is a plot of double homoclinic solutions with  $\varepsilon = 0.076071148687$ .

(ii) Then varying  $\mu \in (0, 0.1)$ , we observe different dynamical phenomenon for Eq.(3.3). We do this by fixing a  $\mu$  value, and varying  $t_0$  over  $[0, 0.1)$  with time step  $\Delta t_0 = 0.001$ . This is to say we observe, from statistical point of view, one thousand solutions for a given  $\mu$  value.

### 3.2.2. Simulation results

Let  $\omega = 2\pi$ . Our simulation results, for all values of  $\mu$ , return one of the following dynamical phenomena.

(I) Periodic sinks. We observe Fig.3 at  $\mu = 3 \times 10^{-4}$  and  $t_0 = 0$ , which is a periodic sink representing stable dynamics of equation (3.3). The horizontal lines in part(c)

show that the discrete orbit plotted in part (a) is indeed a periodic orbit. Part (b) is the projection of part (a) on  $x - y$  plane. Since Eq.(3.1) has two homoclinic solutions, we have two cases of periodic sinks: two-sided periodic sink going around the two homoclinic solutions in Fig.3, and one-sided periodic sink staying around one of the two homoclinic solutions in Fig.4.

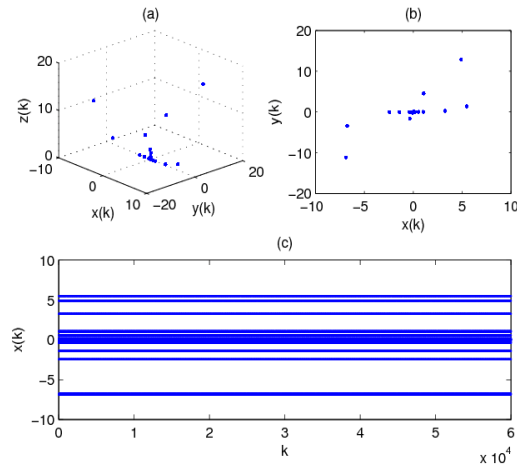


Figure 3. Two-sided periodic sink for equation (3.3) at  $\mu = 3 \times 10^{-4}$  and  $t_0 = 0$ . (a) Three-dimensional phase portrait; (b) Projection on  $x - y$  plane; (c) Time evolution of  $x(t)$ .

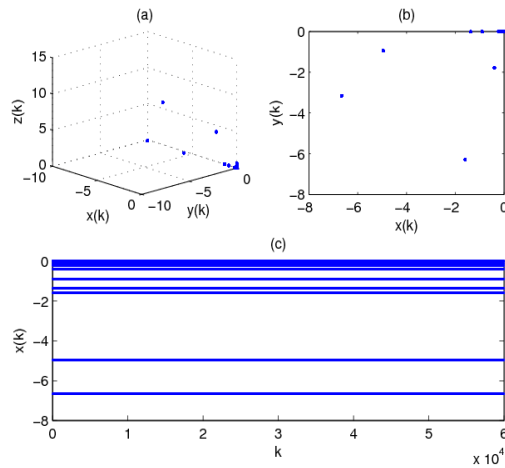


Figure 4. One-sided periodic sink for equation (3.3) at  $\mu = 1.780 \times 10^{-5}$  and  $t_0 = 0$ . (a) Three-dimensional phase portrait; (b) Projection on  $x - y$  plane; (c) Time evolution of  $x(t)$ .

(II) Hénon-like attractors. The plots returned are as in Fig.5 and Fig.6. They

are strange attractors with invariant SRB measures, representing chaotic behaviors around periodic solutions. The time evolution in part (c) displays the stochastic distribution of orbits. Part (d) is the continuous Fourier spectrum.

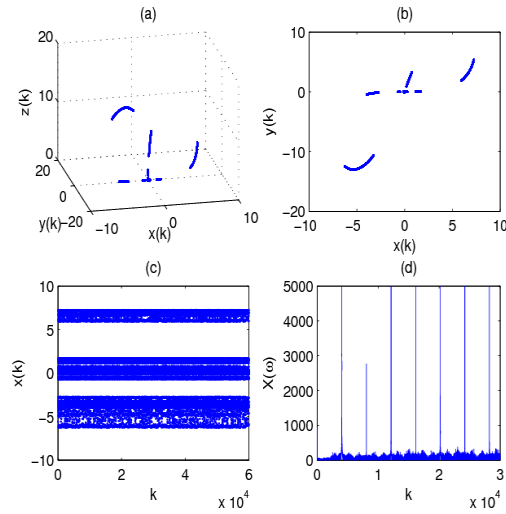


Figure 5. Two-sided Hénon-like attractors for equation (3.3) at  $\mu = 5 \times 10^{-4}$  and  $t_0 = 0$ . (a) Three-dimensional phase portrait; (b) Projection on  $x - y$  plane; (c) Time evolution of  $x(t)$ ; (d) Fourier spectrum of  $x(t)$ .

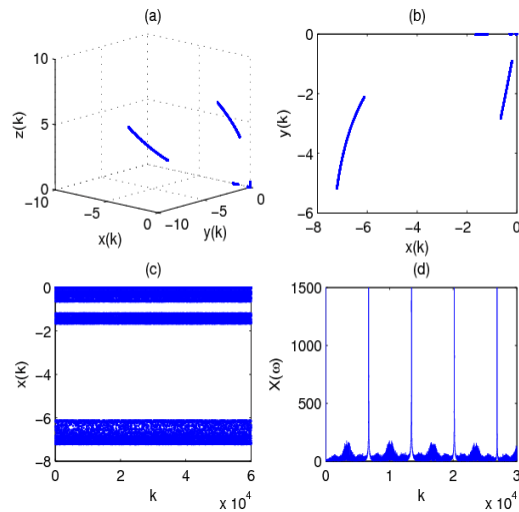


Figure 6. One-sided Hénon-like attractors for equation (3.3) at  $\mu = 3.307 \times 10^{-5}$  and  $t_0 = 0$ . (a) Three-dimensional phase portrait; (b) Projection on  $x - y$  plane; (c) Time evolution of  $x(t)$ ; (d) Fourier spectrum of  $x(t)$ .

(III) Rank one attractors. Figure 7 is the rank one attractor observed at  $\mu = 1.211 \times 10^{-4}$  and  $t_0 = 0$ . Part (a) is the phase portrait in three-dimensional space. Although it looks like part (a) in Fig.1, they are critically different from the time evolution in part (c). Rank one attractor is chaotic with good mixing properties. It is an invariant set with a basin of positive Lebesgue measure. Though every orbit from its basin behaves randomly, it converges to a uniformly distribution dedicated by a global SRB measure. Part (b) is the projection of part (a) on  $x - y$  plane. Part (d) is the continuous Fourier spectrum of  $x(t)$ .

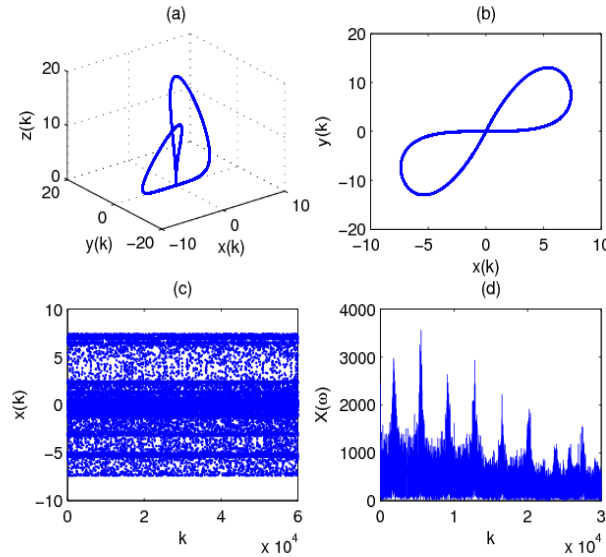


Figure 7. Rank one attractors for equation (3.3) at  $\mu = 1.211 \times 10^{-4}$  and  $t_0 = 0$ . (a) Three-dimensional phase portrait; (b) Projection on  $x - y$  plane; (c) Time evolution of  $x(t)$ ; (d) Fourier spectrum of  $x(t)$ .

For varied  $\mu \in (0, 0.1)$ , all simulation results are tabulated in Table 1. We list out the transient values of  $\mu$  from one dynamical phenomenon to another. The symbols “R2”, “S1”, “S2”, “HL1”, “HL2” stand for two-sided rank one attractors, one-sided periodic sinks, two-sided periodic sinks, one-sided Hénon-like attractors, and two-sided Hénon-like attractors. For two effective digits, there are 12 cases in one dynamical pattern. From table 1, the actual ratio meets well with the theoretical period  $e^\beta \approx 6.0496$ , where  $\beta$  is the unstable eigenvalue of saddle  $O(0, 0, 0)$ .

## 4. Conclusion

Three types of attractors present in a periodically perturbed Lorenz-like equation: Hénon-like attractors, rank one attractors, and periodic sinks. They form a fixed pattern repeating with certain period, and are observed in numerical simulations. The results are in perfect harmony with the two-dimensional homoclinic tangle theory, and will push the three-dimensional homoclinic tangle theory forward.

## Acknowledgement

The authors would like to thank Professor Jibin Li for his generous support. Our thanks also extend to Professor Qiudong Wang for his advice on numerical simulations.

## References

- [1] A. Arneodo, P. Coulet and C. Tresser, *A possible new mechanism for the onset of turbulence*, Physics Letters A 81(1981),197-201.
- [2] M. Benedicks and L.-S. Young, *Sinai-Bowen-Ruelle measure for certain Hénon maps*, Invent.Math. 112(1993),541-576.
- [3] V. Carbone, G. Cipparrone and G. Russo, *Homoclinic gluing bifurcations during the light induced reorientation in nematic-liquid-crystal films*, Phys.Rev.E. 63(2001),051701.
- [4] F.J. Chen, A.Oksasoglu and Q.D. Wang, *Heteroclinic tangles in time-periodic equations*, J.Differ.Equ. 254(2013),1137-1171.
- [5] Q.D. Wang and A. Oksasoglu, *Dynamics of homoclinic tangles in periodically perturbed second-order equations*, J.Differential Equations, 250(2011),710-751.
- [6] Q.D. Wang and A. Oksasoglu, *Periodic occurrence of chaotic behavior of homoclinic tangles*, Physica D: Nonlinear Phenomena 239(2010),387-395.
- [7] Q.D. Wang, *Periodically forced double homoclinic loops to a dissipative saddle*, Preprint.
- [8] L.-S. Young, *What are SRB measures, and which dynamical systems have them?* J.Stat.Phys. 108(2002),733-754.

$\beta=1.8, \alpha=1.5, \delta=-0.07$		
$\varepsilon=0.076071148687, \omega = 2\pi$		
Theoretical Multiplicity = $e^\beta \approx 6.0496$		
$\mu$	Dynamical behavior	Actual ratio
$9.4 \times 10^{-4}$	R2	-
$7.5 \times 10^{-4}$	HL2	-
$7.3 \times 10^{-4}$	R2	-
$6.5 \times 10^{-4}$	S1	-
$6.4 \times 10^{-4}$	R2	-
$5.1 \times 10^{-4}$	HL2	-
$4.8 \times 10^{-4}$	S2	-
$3.8 \times 10^{-4}$	R2	-
$3.0 \times 10^{-4}$	S2	-
$2.9 \times 10^{-4}$	R2	-
$2.0 \times 10^{-4}$	HL1	-
$1.9 \times 10^{-4}$	S1	-
$1.572 \times 10^{-4}$	R2	5.9796
$1.228 \times 10^{-4}$	HL2	6.1075
$1.211 \times 10^{-4}$	R2	6.0280
$1.077 \times 10^{-4}$	S1	6.0353
$1.074 \times 10^{-4}$	R2	5.9590
$8.445 \times 10^{-5}$	HL2	6.0390
$7.925 \times 10^{-5}$	S2	6.0567
$6.423 \times 10^{-5}$	R2	5.9162
$4.968 \times 10^{-5}$	S2	6.0386
$4.698 \times 10^{-5}$	R2	6.1728
$3.309 \times 10^{-5}$	HL1	6.0441
$3.229 \times 10^{-5}$	S1	5.8841
$2.604 \times 10^{-5}$	R2	6.0407
$2.030 \times 10^{-5}$	HL2	6.0462
$2.002 \times 10^{-5}$	R2	6.0489
$1.780 \times 10^{-5}$	S1	6.0449
$1.777 \times 10^{-5}$	R2	6.0438
$1.395 \times 10^{-5}$	HL2	6.0537
$1.311 \times 10^{-5}$	S2	6.0450
$1.060 \times 10^{-5}$	R2	6.0594
$8.216 \times 10^{-6}$	S2	6.0460
$7.769 \times 10^{-6}$	R2	6.0471
$5.472 \times 10^{-6}$	HL1	6.0471
$5.329 \times 10^{-6}$	S1	6.0693
$4.307 \times 10^{-6}$	R2	6.0459
$3.356 \times 10^{-6}$	HL2	6.0488
$3.309 \times 10^{-6}$	R2	6.0502
$2.943 \times 10^{-6}$	S1	6.0483
$2.939 \times 10^{-6}$	R2	6.0462
$2.306 \times 10^{-6}$	HL2	6.0494
$2.171 \times 10^{-6}$	S2	6.0387
$1.752 \times 10^{-6}$	R2	6.0502
$1.358 \times 10^{-6}$	S2	6.0501
$1.284 \times 10^{-6}$	R2	6.0506
$9.047 \times 10^{-7}$	HL1	6.0484
$8.810 \times 10^{-7}$	S1	6.0465

Table 1. The periodic pattern of equation (3.3)